TÜBİTAK

Turkish Journal of Earth Sciences

http://journals.tubitak.gov.tr/earth/

Research Article

Turkish J Earth Sci
(2017) 26: 170-188

doi:10.3906/yer-1608-18

Terrestrial-marine sedimentary cycles in the South Yellow Sea, China: implications for paleoenvironmental reconstruction since MIS 5

Liangtao YE[1,2,3], Ge YU[1,*], Mengna LIAO[1], Shouyun HU[1], Longsheng WANG[1], Lei GAO[1]

[1]State Key Laboratory of Lake Science and Environment, Nanjing Institute of Geography and Limnology, Chinese Academy of Sciences, Nanjing, P.R. China

[2]College of Environmental Science and Engineering, Anhui Normal University, Wuhu, P.R. China

[3]University of Chinese Academy of Sciences, Beijing, P.R. China

Received: 31.08.2016 • **Accepted/Published Online:** 05.04.2017 • **Final Version:** 15.06.2017

Abstract: Sedimentary records of the continental shelves since Marine Isotope Stage (MIS) 5 are valuable for paleoenvironmental reconstruction and decipherment of land–sea interactions. Since the 1990s, different perspectives on global glacioclimate magnitudes and the associated evolution of major sedimentary environments during the Late Pleistocene have caused a distinctive understanding of marine transgressions and coastal deposits during MIS 3 and MIS 5. Moreover, the chronology of sediment sequences from this region was primarily determined based on radiocarbon dating, which might be problematic for deposits of 40–50 ka BP or older. In this study, we used both a 150-m-long sedimentary core (YZ07) as a typical record and 12 collected regional boreholes as a synthesis to resolve the issues. On the basis of an age model of accelerator mass spectrometry (AMS) radiocarbon and optically stimulated luminescence (OSL) dating, the sedimentary sequences during the period from MIS 5 up to MIS 1 were documented by Core YZ07 drilled from the western coast of the South Yellow Sea (SYS), and the marine sediments were recognized by the paleontological fossils. The results indicate three terrestrial-marine sedimentary cycles since MIS 5, including the MIS 5, MIS 3, and MIS 1 marine transgressions as well as the MIS 2 and MIS 4 marine regressions in the coastal plain and offshore area of the SYS. Meanwhile, there was a major sedimentary hiatus during MIS 2 and MIS 4 due to strong erosions. Different dating methods on these regional cores, including AMS ^{14}C and OSL, have confirmed the existence of the MIS 3 marine transgression in the SYS. The intensity of marine transgression and the height of sea levels during MIS 3 and MIS 5 recorded in sediments were dominated by the changes of global climate-driven glaciers and regional tectonic movement.

Key words: Sedimentary cycles, paleontological fossils, MIS 5, stratigraphic sequence, marine transgression, South Yellow Sea

1. Introduction

The continental shelves are transitions between continents and oceans, and they are vital to acquire the information on land–sea interactions and associated climate changes and sea-level fluctuations (Wang, 1998; Yao et al., 2012). The continental shelf in the South Yellow Sea (SYS) was once a coastal plain during the Late Pleistocene, on which filled huge quantities of sediments from the old Yangtze River and Yellow River (Wang, 1998). Therefore, a radial sand ridge field that was referred to as an estuary-delta sedimentary system of the Yangtze was developed on the continental shelf of the SYS during the Holocene (Ren, 1986; Wang, 1998; Wang et al., 2012). The old Yellow River Delta and the old Yangtze Delta have governed and influenced the sand ridge fields since the Holocene (Ren, 1986; Wang, 2002; Wang et al., 2012; Gao and Collins, 2014). In addition, the global climate has gone through several interglacial-glacial climatic cycles since the Late Pleistocene, including the last interglacial, last glacial, and postglacial periods (Lowe and Walker, 1997; Lisiecki and Raymo, 2005). Subsequently, a range of glacioeustatic sea-level fluctuations occurred in response to interglacial–glacial climatic cycles, respectively. Therefore, the radial sand ridge fields and underlying continental shelf have experienced several transgressive and regressive cycles since the Late Pleistocene, which led to interbedded marine and terrestrial sediments in coastal zones (Chen, 1957; Ren, 1986; Wang, 2002, 2014; Wang et al., 2012).

Compared with sea-level lowstands during Marine Isotope Stage (MIS) 2 and MIS 4, at least three major marine transgression events were reported in the coastal plains of the SYS since the Late Pleistocene, termed the Zhenjiang transgression during MIS 1 (Lin et al., 1989), the Gehu transgression during MIS 3 (Lin et al., 1989), and the Taihu transgression during MIS 5 (Wang et al., 1981). The fitting curve of sea level in the SYS is approximately

* Correspondence: geyu@niglas.ac.cn

consistent with the global sea-level curve since MIS 5 and the highest sea levels during MIS 5 are higher than MIS 3 ones (Wang and Wang, 1980; Chappell and Shackleton, 1986). The highest sea levels during MIS 5 were estimated to be –11 to 10 m average sea level (a.s.l.) along the worldwide coasts (Steinen et al., 1973; Chappell, 1974; Chappell and Veeh, 1978; Murray-Wallace, 2002; Simms et al., 2009), while the highest sea levels during MIS 3 were estimated to be –15 to –10 m a.s.l. on the West Pacific coasts around Japan and New Guinea (Chappell and Shackleton, 1986; Fuji and Horowitz, 1989; Shi et al., 2001) and to be –10 to –5 m a.s.l. in the Chinese marginal seas (Wang and Wang, 1980; Huang et al., 1986; Shi and Yu, 2003; Zhao et al., 2008), respectively.

Ambiguity concerning the MIS 3 and MIS 5 transgressions in the SYS centers on two issues. The first is on whether the MIS 3 transgression did take place in the SYS. In the past decades, some workers stated that the previously radiocarbon-dated MIS 3 transgression was virtually optically stimulated luminescence (OSL)-dated back to MIS 5 (Yim et al., 1990; Simms et al., 2009; Yi et al., 2013). The chronology of previous studies on the SYS sediments is mostly determined by radiocarbon dating, which is constrained within 35–45 ka BP owing to its radioactive half-life limit (Long and Shen, 2015). The upper limit of OSL dates can extend to 1×10^5–7×10^5 ka BP depending on samples (Lai et al., 2014). Radiocarbon dating was thus considered as unreliable compared with OSL dating for deposits of >40–50 ka BP (Yim et al., 1990; Yi et al., 2013). OSL dating has already been proven to be a robust dating method for coastal and marine sediments all over the world (e.g., Jacobs, 2008; Sugisaki et al., 2010; Kim et al., 2015). The second is the mechanism of transgression during MIS 3 and MIS 5 in the SYS. Sediment records in the coastal area of the SYS showed that the MIS 3 marine transgression deposits were found to be significant (Wang et al., 1981; Lin et al., 1989; Zhao et al., 2008; Zhang et al., 2010; Wang et al., 2013), while the records of the transgression sediments during MIS 5 seemed to be sporadic (Wang et al., 1981; Zhao et al., 2008). Since the sea levels during MIS 5 were considered to be higher than MIS 3 ones (Chappell and Shackleton, 1986), why did the sedimentary records in the SYS suggest that transgression during MIS 3 was generally more significant than that during MIS 5 (Wang et al., 1981)?

In order to generate more evidence correlating paleoenvironmental evolution in the SYS since MIS 5, a 150-m-long core (YZ07) was drilled in the Jiangsu coast of the SYS. Radiocarbon and OSL dating were measured, and analyses of foraminifera, diatoms, and mollusks were conducted on the sediment samples in Core YZ07. Previously published stratigraphic and chronological data from 12 cores in the delta area and adjacent continental shelf were also analyzed (Figure 1). This study intends to reconstruct paleoenvironmental changes in the deltaic plain and offshore area of the SYS from MIS 5 up to MIS 1 and to understand the possible mechanisms of marine transgression during MIS 3 and MIS 5.

2. Regional setting

The Yellow Sea is a typical semienclosed epicontinental sea bounded by the Chinese Continent and Korean Peninsula. It rests on a flat, broad, and tectonically stable seafloor with water depth of average 55 m and maximum 100 m (Yang et al., 2003). The Yellow Sea is separated from the East China Sea to the south by a line connecting the north margin of the Yangtze River mouth with Cheju Island, and from the Bohai Sea to the west by the Bohai Strait. The Shangdong Peninsula separates the SYS from the North Yellow Sea. The SYS and North Jiangsu basin, tectonically connected and integrated, is a Cenozoic basin, which formed a united sedimentary basin during the Neogene period (Bureau of Geology and Mineral Resources of Jiangsu, 1984). The SYS has received huge quantities of terrigenous sedimentary inputs from the nearby landmass of China since the Quaternary via many rivers, mainly including the large rivers of the Yangtze and the Yellow. Therefore, some 300-m unconsolidated sediments in the coastal plains of the SYS have been accumulated since the Quaternary, and massive sediments also resulted in the development of the aggradational continental shelf of the SYS (Wang et al., 2006). The Yangtze River once flowed into the SYS through the middle of the present Jiangsu coast, and the old Yellow River also flowed into the SYS repeatedly through the present Jiangsu coast in geological history. Therefore, these two large rivers are the origin of the main terrigenous clastics of the Jiangsu coastal area (Ren, 1986; Wang et al., 2006). The modern Jiangsu coast has strong tidal currents with a well-developed tidal-flat system and a massive magnitude of tidal-flat deposits (Wang et al., 2012; Gao, 2013; Wang et al., 2014).

The depositional system of the SYS and paleo-Yangtze delta consists of interbedded terrestrial and marine sediments in response to the Late Pleistocene climate cycles and associated periodic sea-level fluctuations. The depositional system of the paleo-Yangtze delta, defined by the present-day Jiangsu coast and the 40-m isobaths in the SYS, formed in the paleo-valley during MIS 6 to MIS 4 (Lin et al., 2015). Subsequently, the depositional systems of delta and onshore aggradations were developed during MIS 3. Since the mid-MIS 3, major river channels in the Yangtze delta area have shifted southward, so the early-formed southern delta area has developed into incised paleo-valley geomorphology (Wang et al., 2006; Wang et al., 2008; Wang, 2014; Zhang et al., 2010). The Yangtze River alternated its outlet to the present-day river mouth

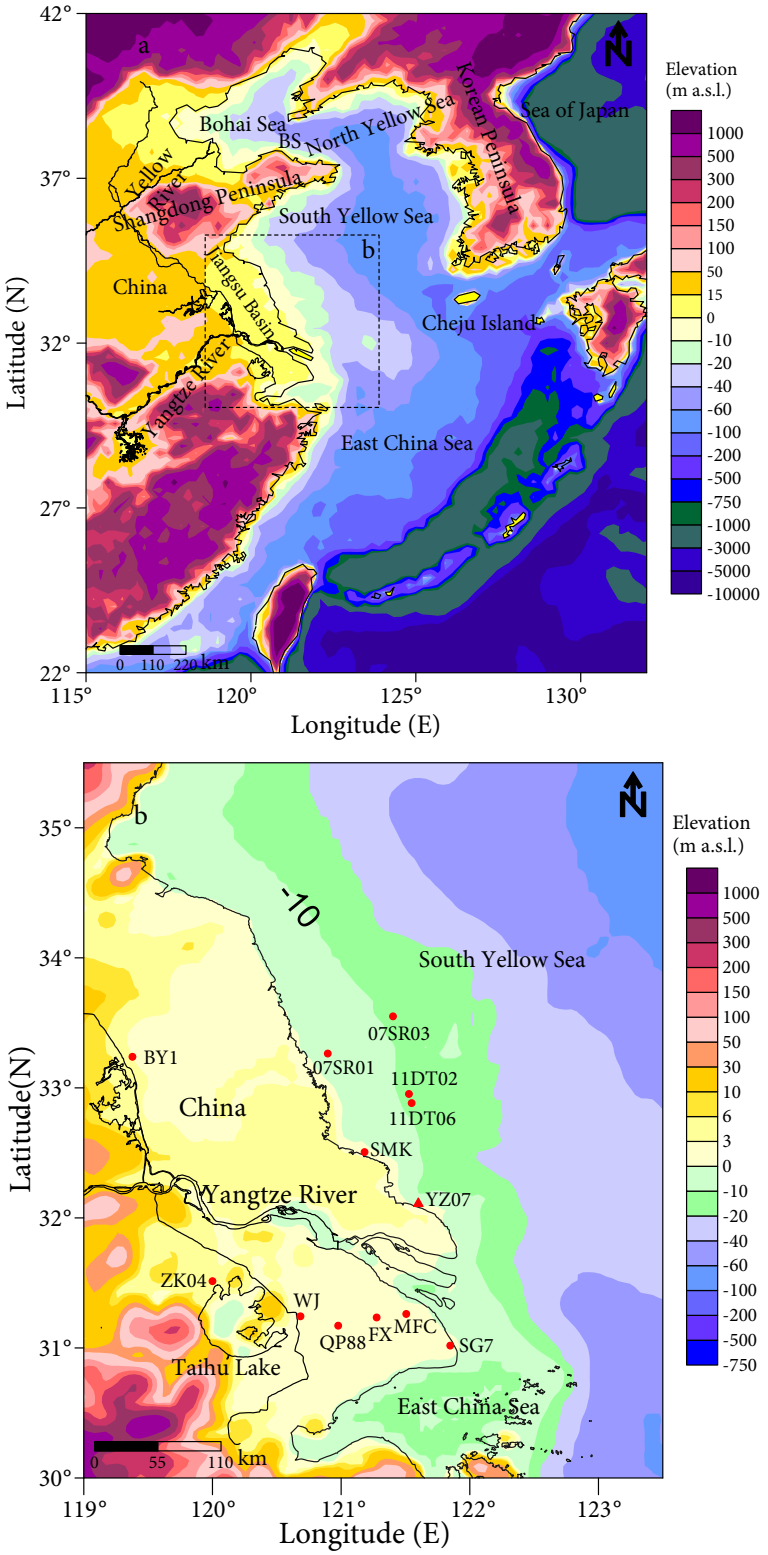

Figure 1. Geographic map of the study area. (a) Schematic map of the bathymetry in the Yellow Sea and adjacent areas. (b) Locations of the sedimentary cores in the continental shelf of the SYS and adjacent coastal plains. Core references: 07SR03 (Zhang et al., 2014); 07SR01 (Xia et al., 2013); 11DT02 (Li et al., 2013); 11DT06 (Wang et al., 2014); SMK (Zhu et al., 1999); BY1 (Zhang et al., 2010); ZK04 (Zhong et al., 1999); WJ (Wang et al., 2013); QP88 (Wang et al., 2013); FX (Zhao et al., 2008); MFC (Zhao et al., 2008); SG7 (Wang et al., 2013); YZ07 (this study). Red triangle denotes YZ07 in this study; red dots denote cores in previous studies; BS denotes Bohai Strait.

during the Holocene, so a large-scale tidal-flat depositional system has been formed in the western SYS.

3. Materials and methods

Core YZ07(32.084°N, 121.797°E) was drilled in the tidal-flat area with the elevation of –2 to –5 m off the shore of Dongzao harbor on the Jiangsu coast in 2007 (Figure 1). The total penetration depth of the core is 150 m and its recovered length is 143.44 m, illustrating that the total recovery rate is 95.6%.

In the laboratory, the core was split lengthwise and visually described, including the sediment color, grain size, sedimentary textures, sedimentary structures, erosional boundary, and paleontological fossils. Subsamples were taken according to the variation of lithology, including 1333 subsamples for grain-size analysis, 54 subsamples for foraminifer identification, 178 subsamples for diatom identification, 24 subsamples for bivalve and gastropod identification, 14 subsamples for radiocarbon-14 dating, and 9 subsamples for OSL dating.

3.1. Grain-size measurement

Analyses of grain size were carried out at the Nanjing Institute of Geography and Limnology, Chinese Academy of Sciences. Before measuring grain size, samples were pretreated with 10% H_2O_2 and 0.1 N HCl to remove organic matter and biogenic carbonate. Grain-size analysis of the <2 mm particles was carried out on a Malvern Mastersizer 2000 laser particle size analyzer. Particles of >2 mm were determined using the sieving method. Measurements by the two methods were integrated to get the whole grain-size distribution.

3.2. Paleontological fossil identification

For foraminifer analysis, standard treatment methods were used and the fraction of >63 μm was examined. Results were recalculated on the basis of the wet sample weight of 100 g. Mollusk shells in the cores were picked out and identified. For diatom analysis, sample treatment and preparation of quantitative slides by light microscopy followed the standard procedure (Gersonde and Zielinski, 2000), and the counting method was according to Schrader and Gersonde (1978). At least 300 diatom valves were counted per sample using a Nikon microscope at 1000× magnification. Diatom identification was completed at the Nanjing Institute of Geography and Limnology, Chinese Academy of Sciences. Foraminifer samples were identified at Zhejiang Ocean University. Bivalve and gastropod identification was performed at the Nanjing Institute of Geology and Paleontology, Chinese Academy of Sciences.

3.3. Radiocarbon and OSL dating

Radiocarbon-14 dating was mainly conducted on mollusk shells, plant debris, and organic-rich clay using an accelerator mass spectrometry (AMS) system at the GNS Rafter Radiocarbon Laboratory in New Zealand. All radiocarbon age determinations were calibrated by using Calib Ver. 5.0.1 (http://calib.qub.ac.uk) with one standard deviation (1σ) of uncertainty.

All OSL sample preparations and luminescence measurements were conducted at the Luminescence Dating Laboratory of NIGLAS (Nanjing, China). In the luminescence laboratory, the sediments at each end of the cylinders were scraped off for dose rate determination and the unexposed light sediments in the middle part of the cylinder were used for equivalent dose (De) determination. The materials were first wet-sieved to obtain the coarse-grained fraction (CG, 90–200 μm), followed by treatment with 30% H_2O_2 and 10% HCl to remove any organic matter and carbonates, respectively. After that, the quartz-rich fraction was etched with 40% hydrofluoric acid (HF) for 1 h to remove the outer alpha-irradiated layer of the quartz grains and eliminate any feldspar contamination, and then the etched-fraction was rinsed by 10% HCl to remove any fluoride. The pure quartz grains were then mounted onto 10-mm-diameter steel disks by silicone oil adhesive with a 2-mm-diameter monolayer for measurement. OSL measurements were carried out on an automated Risø TL/OSL DA-20 reader equipped with a $^{90}Sr/^{90}Y$ beta source. Quartz OSL signals were stimulated by blue LEDs (470 nm) and detected through a 7.5-mm Hoya U-340 filter. The SAR protocol was used for all OSL measurements (Murray and Wintle, 2000) and the purity of the isolated quartz for each aliquot was examined using the IR depletion in the SAR sequence. The concentrations of uranium (U), thorium (Th), and potassium (K) were measured by the neutron activation analysis. The cosmic ray dose rate was estimated for each sample as a function of depth, altitude, and geomagnetic latitude (Prescott and Hutton, 1994).

3.4. Sedimentary description

On the basis of lithofacies characteristics and downcore distribution of micro- and macrofossils and grain size, the sediments in Core YZ07 can be divided into 14 depositional subunits, designated SU 1–14 in descending order (Figure 2).

SU 1 (150–141.79 m) is primarily composed of bluish green or bluish hard muds with olive gray clayey silt, occasionally containing some gravels, molluscan shell fragments, and plant roots. Abundant freshwater gastropods (*Parafossarulus striatulus* Bensen) were scattered at the core depth of 149 m. The unit is interpreted to have been deposited in a floodplain/lacustrine environment.

SU 2 (141.79–130.16 m) is dominated by light olive gray silt or fine-grained sand with many layers of olive brown clay. The sandy beds display wavy bedding and contain intact spiral shells and some shell fragments. Some gravels and abundant carbonized plant debris are spotted

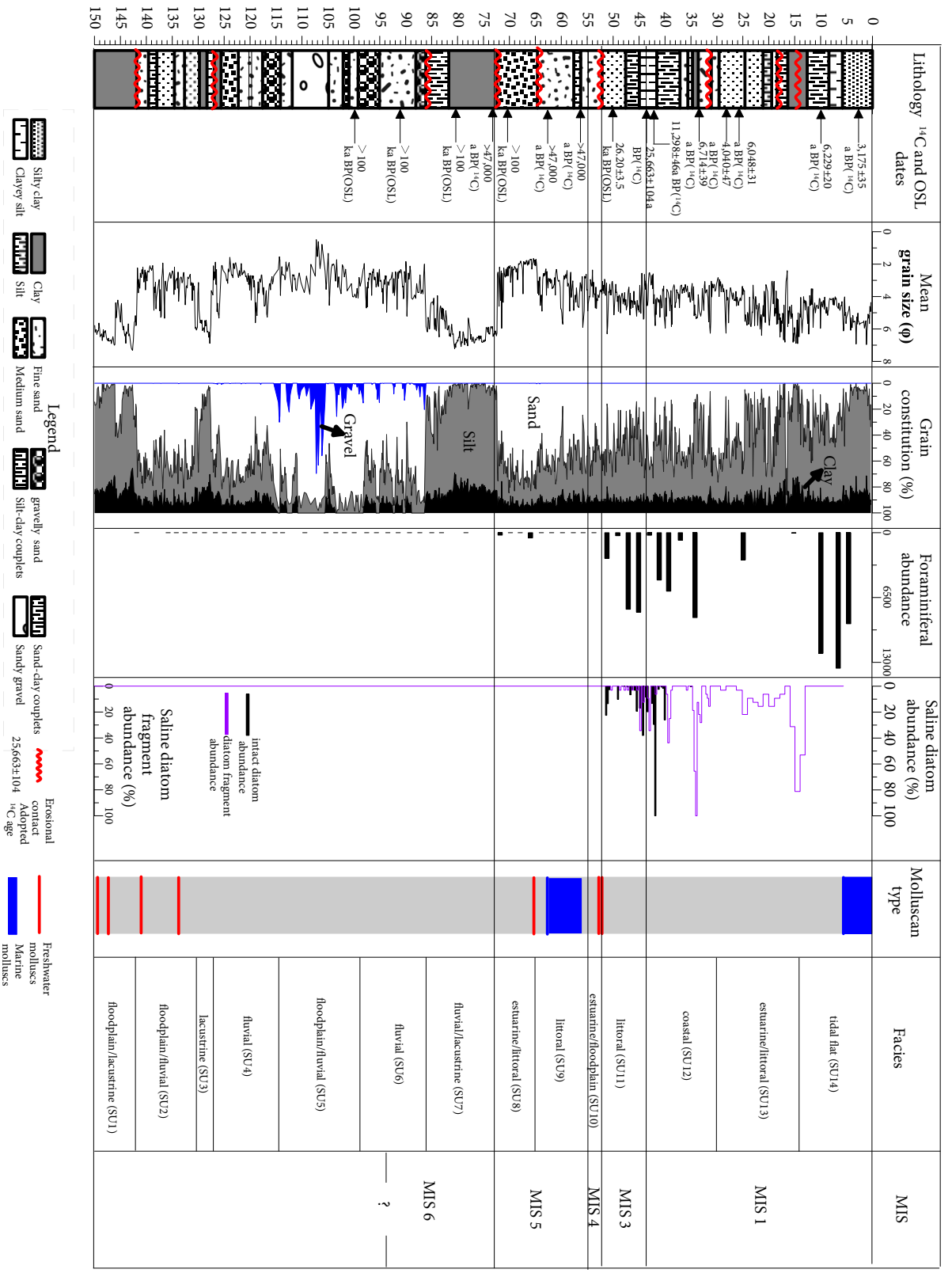

Figure 2. Sedimentary sequence of Core YZ07 with AMS ^{14}C- and OSL-based chronology and the lithology, grain size, saline diatom and foraminiferal abundance, molluscan type, depositional facies, and corresponding MIS divisions.

at the basal section. Freshwater gastropods (*P. striatulus* Bensen) are present at the core depth of 140 m and 134 m. The fine-grained sand beds exhibit an erosional contact with underlying muddy layer. The subunit is interpreted to be a floodplain/estuarine depositional environment.

SU 3 (130.16–126.93 m) is mainly composed of bluish green hard muds with calcareous concretions and some dark brown plant debris. No paleontological fossils are found in this unit, which is interpreted to be a lacustrine deposit.

SU 4 (126.93–114.16 m) has a lower section of mud (125.6–126.93 m) and an upper section of sand (125.6–114.16 m). The upper section of sand is characterized by light olive gray gravel-bearing (6–14 mm in size) fine- to medium-grained sand beds, occasionally containing olive brown silty clay layers (9–15 mm thick) that exhibit lenticular bedding. The lower section of mud is mainly dominated by clay locally with sandy bands, and the bottom shows an erosional contact with underlying unit. Some carbonized plant fragments and brownish red plant debris are locally present. White calcareous concretions are spotted at the core depth of 122.39–124.69 m, which, together with the bottom erosional boundary, suggest that this section was subjected to frequent subaerial exposure and weathering. This subunit is interpreted to have been deposited in a fluvial environment.

SU 5 (114.16–98.16 m) is made up of olive gray fine to coarse sand beds with quartz particles (2–4 mm in size) and mica fragments, occasionally containing thin layers of clay. The sandy beds display horizontal bedding and contain intact spiral shells and mollusk shell fragments. The bottom section consists of olive gray sandy gravel bands with subrounded or subprismatic pebbles (15–70 mm), locally containing carbonized plant fragments and brownish red plant debris. Hence, this subunit is interpreted as a floodplain/fluvial deposit.

SU 6 (98.16–86.10 m) is primarily composed of olive gray fine- to coarse-grained sand, locally intercalated with olive brown clay bands. The sandy beds locally display faint horizontal lamination but obvious oblique bedding, and are sporadically scattered with quartz particles, mica debris, dark silt-class minerals, and plant debris. No paleontological fossils are found in this subunit. This subsection is interpreted as a fluvial depositional environment.

SU 7 (72.10–86.10 m) is dominated by olive brown or brown hard muds, interlaminated with light olive gray silty beds scattered with lenses at the basal section, which exhibits an erosional contact with the underlying sandy sediments. Lamination is almost absent in this subunit. Yellowish brown mottles and iron manganese concretions (1–3 mm) are scattered. The subunit is interpreted to have been deposited in a fluvial/lacustrine environment.

SU 8 (72.10–64.60 m) mainly consists of light olive gray or light gray medium- to fine-grained sand, locally interbedded with thin clay layers with faint wavy bedding. Quartz particles (5 mm), freshwater mollusk shells and fragments, concretions, and carbonized plant debris are sporadically scattered. There is an abundance of 245–517 foraminiferal individuals/50 g dry sediment in this section. The basal section exhibits an erosional contact with the underlying muddy layer. The subunit is interpreted to have been deposited in an estuarine/littoral environment.

SU 9 (64.60–54.98 m) is dominated by light olive gray fine sand, occasionally intercalated with silty beds with horizontal wavy-bedding, locally containing millimeter-scale layers of clayey silt to fine-grained sand. The bottom section exhibits an erosional contact with the underlying layer. The gastropod assemblages at the core depth of 55.8 to 62.8 m are dominated by littoral species, including *Gyraulus albus*, *Parabithynia lognicornis*, and *Turbonilla* cf. *nonnota* Nomuta. This subunit is interpreted to have been deposited in a littoral environment.

SU 10 (54.98–52.16 m) is primarily composed of light olive gray fine-grained sand with a few gravels, intercalated with beds of olive brown clayey silt and millimeter-scale layers of olive brown clay (4–18 mm). The sandy beds display wavy lamination and contain iron manganese concretions (5–7 mm), a single spiral shell (5 mm × 8 mm), and quartz particles (<1.5 mm). Abundant little white spiral shell fragments occur at the basal section. A species of freshwater gastropod (*P. striatulus* Bensen) was spotted at the core depth of 52.8 m. The top boundary shows an erosional contact with overlying silty layer. The subunit is interpreted to have been deposited in a fluvial/floodplain environment.

SU 11 (52.16–43.88 m) has a lower section of sand (52.16–48.97 m) and upper section of clayey silt to silt (48.97–43.88 m). The sandy section consists of olive gray fine-grained sand beds (5–20 mm) interbedded with thin layers of olive brown clay (3–5 mm thick) with wavy bedding. The silty section is dominated by clayey silt to silt, locally interlaminated with thin bands (8–15 mm thick) of light olive brown clay. Saline diatom fossils are present at the core depth of 44.97 to 51.3 m, and the dominant species are *A. mammifer*, *T. nitzschioides*, *Thalassirothrix* spp., *T. excentrica*, and *Xanthiopyxis* spp. Foraminiferal abundance ranges from 300 to 7967 per 50 g dry sediments at the core depth of 45.70 to 51.05 m, and alien species range from 0.05% to 65.69%, suggesting that this subunit was deposited in a littoral/neritic environment.

SU 12 (43.88–31.75 m) is dominated by olive gray and gray to dark gray silt, locally consisting of clayey silt, interlaminated with centimeter-scale layers of brown gray and olive brown clay, which displays horizontal, flaser, or wavy bedding. The abundance of foraminiferal assemblages

ranges from 749 to 5864 per 50 g dry sediments at the core depth of 35.35 to 41.52 m and a deep-water species (*Epistominella naraensis* Kuwa.) accounts for 1.67%–4.6%. Agglutinated foraminifera begin to appear and the percentage of uniserial test foraminifera begins to increase in the lower part of SU 12, suggesting a deepening-upward sea level. Diatom assemblages at the depth of 38–44 m are dominated by saline species (*C. stylorum/striata*), warm-water species (*C. nodulifer*), and deep-water saline species, including *P. sulcata*, *T. nitzschioides*, *T. excentrica*, and *T. oestrupii*. It is interpreted to have been deposited in a coastal environment.

SU 13 (31.75–14.71 m) mainly consists of light brown clayey silt to fine-grained sand and silty clay, interbedded with brown gray clay beds with occasional burrows. This subunit displays an obvious erosional contact with the underlying strata, which is suggestive of an estuarine or littoral process. Some beds show centimeter-scale alternations of clay (12–25 cm thick) and sand (12–19 cm thick). Silty lenses are common in clay beds with silty mottles (8 cm thick) and silty layers (10 cm thick). Prominent sedimentary structures include cross-bedding and graded bedding suggestive of tidal action. The subunit is sporadically scattered with abundant shell and mica debris, dark silt-scale minerals, plant roots and plant debris. The foraminiferal abundance averages from 34 to 2723 individuals per 50 g dry sediments at the core depth of 14.85 to 24.89 m, and a deep-water species (*E. naraensis* Kuwa.) accounts for 4.94%–31.08%. There are also some saline diatom fragments in this section. SU 13 is interpreted to have been deposited in a littoral/estuarine environment.

SU 14 (14.71–0 m) is made up of light olive gray clayey silt and taupe brown clay bands or mottles, interlaminated with gray brown clay, exhibiting abundant flaser or cross-bedding, and contains abundant saline diatom fragments suggestive of tidal action. A lot of plant debris and plant roots are present at the core depth of 8.9–8.6 m. Planktonic foraminifer assemblages (*E. naraensis* Kuwa. and *U. canariensis*), suggesting that they were carried into the SYS by warm currents from the open sea, reach a peak at the core depth of 0 to 6 m. Moreover, bivalve species (*M. meretrix* Linnaeus), indicative of modern littoral environments, are also present. The bottom section exhibits an erosional contact with the underlying silt/clay band. This subunit demonstrates a tidal-flat depositional environment.

4. Results

4.1. Age model of Core YZ07

The chronology in Core YZ07 was built by radiocarbon and OSL dating. Fourteen sediment samples from the borehole Core YZ07 were dated by AMS ^{14}C dating (Table 1). Based on stratigraphy analysis, we discarded some dates such as "age too young" (ATY) (Webb, 1985) in that sample materials were from a single spiral shell, or "age too old" (ATO) in that the samples were from black organic-rich clay. The age inversions of the core stratigraphic sequence may be attributed to admixtures of younger carbon (ATY) or older carbon (ATO) because of complex coastal transport and reworked depositions, so the reliability of these sample radiocarbon age determinations is questioned (Wang et al., 1998). After excluding these unreliable datings, the ages of sediments can illustrate the late Pleistocene stratigraphic sequence in the study area. Therefore, ages of 3175 ± 35 cal. a BP, 6229 ± 20 cal. a BP, 6048 ± 31 cal. a BP, 4040 ± 47 cal. a BP, 6714 ± 39 cal. a BP, 11,298 ± 46 cal. a BP, 25,663 ± 104 cal. a BP, and >47,000 cal. a BP were adopted after evaluating the regional stratigraphy (Table 1). The OSL dates of sediments at the core depths of between 6.4 and 100 m show ages of 1.2 ± 0.1 ka BP, 3.3 ± 0.5 ka BP, 3.7 ± 0.5 ka BP, 6.2 ± 1.0 ka BP, 26.2 ± 3.5 ka BP, and >100 ka BP, respectively (Table 2).

Overall, the burial depth boundaries and geological eras since 128 ka BP (equivalent to MIS 5) during the Late Pleistocene can be divided into 4 subunits. The boundaries of MIS 5/6, MIS 4/5, MIS 3/4, and MIS 1/2 in YZ07 occurred at the core depths of 72.1 m (128 ka BP), 54.98 m (75–70 ka BP), 52.16 m (55–60 ka BP), and 41.6 m (1.2–1.0 ka BP), respectively.

4.2. Paleontological analysis

4.2.1. Bivalve and gastropod identification

Assemblages of bivalves and gastropods, indicative of freshwater or saline environments, were identified from various layers of Core YZ07 (Table 3). Saline bivalve and gastropod assemblages are only present in two layers. Saline bivalve species, such as *Meretrix meretrix* Linnaeus, are dominant at the core depth of 0 to 6 m, reflecting littoral and/or intertidal environments (labeled MT 1). The gastropod assemblages at the core depth of 55.8 to 62.8 m are dominated by saline species, including *Gyraulus albus* Müller, *Parabithynia lognicornis* Benson, and *Turbonilla* cf. *nonnota* Nomuta. The assemblage is interpreted to reflect littoral and/or tidal-flat environments, equivalent to the MIS 5 marine transgression stage (labeled MT 3). Meanwhile, the gastropod assemblages at the core depths of 51–52 m and 131.4–147.8 m are dominated by freshwater species, such as *Parafossarulus striatulus* Bensen, and abundant freshwater bivalve fragments are also scattered at the core depth of 131.4 to 147.8 m, indicating fluvial/lacustrine depositional environments.

4.2.2. Diatom identification

Diatom fossils are only distributed at the core depth of 0 to 51.3 m (Figure 2). Generally, freshwater diatom shells are easily subjected to corrosions in seawater with high

Table 1. List of AMS-^{14}C dating from Core YZ07 in this study.

Lab no.	Depth (m)	Materials	Conventional ^{14}C age (a BP)	Calibrated ^{14}C age (cal. a BP with 1σ)	Note
NZA-57505	–2.62	Plant debris	2985 ± 25	3175 ± 35	Adopted
NZA-57506	–5.87	Organic-rich clay	7601 ± 31	8398 ± 15	ATO
NZA-57507	–9.9	Plant debris	5421 ± 27	6229 ± 20	Adopted
NZA-57508	–16.52	Organic-rich clay	13,353 ± 47	16,069 ± 94	ATO
NZA-57509	–19.51	Organic-rich clay	24,482 ± 137	28,593 ± 158	ATO
NZA-57510	–25.84	Plant debris	5323 ± 27	6048 ± 31	Adopted
NZA-57903	–28.53	Shell fragments	4034 ± 19	4040 ± 47	Adopted
NZA-57904	–33.67	Shell fragments	6271 ± 22	6714 ± 39	Adopted
NZA-57984	–42.96	Shell fragments	9926 ± 34	11,298 ± 46	Adopted
NZA-59472	–43.88	Shell fragments	21,311 ± 91	25,663 ± 104	Adopted
NZA-59046	–56.06	Plant debris	>47,000		Adopted
NZA-59047	–62.82	Plant debris	>47,000		Adopted
NZA-59163	–72.28	Plant debris	>47,000		Adopted
NZA-59473	–84.67	Single spiral shell	26,788 ± 172	30,946 ± 118	ATY

ATO denotes age too old; ATY denotes age too young; lab numbers are international numbers of the GNS Rafter Radiocarbon Laboratory in New Zealand.

Table 2. List of OSL dates from Core YZ07 in this study.

Lab. no.	Depth (m)	Materials	Equivalent dose (Gy)	OSL age (ka BP)
NL-588	–6.4	Clayey silt	2.24	1.2 ± 0.1
NL -603	–22.1	Silty clay	6.64	3.3 ± 0.5
NL -612	–30.3	Fine sand	7.30	3.7 ± 0.5
NL -626	–44.4	Clayey silt	11.88	6.2 ± 1.0
NL -632	–50.3	Silty clay	43.49	26.2 ± 3.5
NL-642	–70.4	Fine/medium sand	>300	>100
NL-652	–80.1	Clayey silt	>300	>100
NL-672	–91.2	Fine sand	>300	>100
NL-681	–100.0	Fine silt	>300	>100

salinity and high alkalinity. That may be why they are hard to be preserved in the bottom section. Furthermore, saline diatom individuals are only found at the top section of 0 to 6.5 m and at the core depth of 35.0 to 51.3 m (Figure 3). Saline diatom assemblages from the uppermost 6.5 m are dominated by benthic, nearshore, or intertidal species, i.e. *Actinoptyclus ingens*, *A. octonarius*, and *Delphineis/Raphineis surirella*. There are also a few *A. mammifer*, *Thalassirothrix excentrica*, *T. nitzschioides*, and *T. nitzschioide*, as well as littoral species such as *A. senerias* (*undulates*), and *A. splenens*. The assemblages illustrate littoral/intertidal environments, corresponding to MT 1 as saline bivalve species indicate. Saline diatom fossils at the core depths of 35–51.5 m are well preserved, indicative of marine sedimentary environments during MIS 3 (labeled MT 2). Saline diatom fossils can be divided into three bands according to species assemblage implications. The assemblages in the first band (50.5–51.5 m) are dominated

Table 3. Occurrence of bivalve and gastropod assemblages and ecological attributes in Core YZ07.

Sample no.	Depth(m)	Species	Species type	Ecological attributes
F-02	–5.91	*Meretrix meretrix* (Linnaeus)	Bivalves	Intertidal (saline)
A-493	–50.85	*Parafossarulus striatulus* (Bensen)	Gastropods	Freshwater
F-11	–52.21	*Parafossarulus striatulus* (Bensen)	Gastropods	Freshwater
F-15	–62.82	*Parafossarulus striatulus* (Bensen)	Gastropods	Saline
		Gyraulus albus (Müller)		
		Parabithynia lognicornis (Benson)		
		Turbonilla cf. *nonnota Nomuta*		
F-16	–65.39	*Gyraulus albus* (Müller)	Gastropods	Freshwater
F-19	–133.94	*Parafossarulus striatulus* (Bensen)	Gastropods	Freshwater
F-20	–141.11	*Parafossarulus striatulus* (Bensen)	Gastropods	Freshwater
F-21	–147.75	Freshwater bivalve fragments, unidentified species	Bivalves	Freshwater
F-22	–149.66	*Parafossarulus striatulus* (Bensen)	Gastropods	Freshwater

by salt-water species, such as *A. mammifer*, *T. nitzschioides*, *T. excentrica*, and *Xanthiopyxis* spp., especially consisting of *Coscinodiscus nodulifer*, which is susceptible to temperature and salinity changes, reflecting relatively high seawater temperature and sea level at that stage. The assemblages of the second band (44.5–48.5 m) are dominated by *Cyclotella stylorum/striata* and some littoral species, such as *A. senerias/undulates*, *A. splenens*, *A. ingens*, *A. octonarius*, *D./R. surirella*, and *D./R. surirella* var. *australis*. Meanwhile, some salt-water species, *A. mammifer* and *C. nodulifer*, have vanished completely, and the abundances of some salt-water species such as *Paralia* (*Melorira*) *sulcata*, *T. nitzschioides*, *T. excentrica*, *T. oestrupii*, and *Xanthiopyxis* spp. have moderately decreased. The second band is interpreted as the fall of seawater temperature and sea level compared with the first band. The percentage of *C. stylorum*/*striata* decreases slightly in the third band (40–44.5 m), and the abundances of salt-water species *P.* (*M.*) *sulcata*, *T. nitzschioides*, *T. excentrica*, and *T. oestrupii* grow slightly with the reappearance of *C. nodulifer*, indicating a slight increase of seawater temperature and sea level compared with the second band.

4.2.3. Foraminifera identification

Foraminiferal assemblages are only present at the core depth of 0–70.967 m (Figure 4; Table 4). Dominant benthic foraminiferal assemblages are *Ammonia beccarii* vars., *A. convexidorsa*, *A. takanabensis*, *A. compressiuscula*, *Cribrononion porisuturalis*, *C. subincertum*, *Elphidiella kiangsuensis*, *Elphidium advenum*, *E. hispidulum*, *E. magellanicum*, *Hanzawaia nipponica*, *Helenina anderseni*, *Epistominella naraensis*, *Miliammina fusca*, *Bolivina cochei*, *B. robusta*, *Brizalina striatula*, *Bulimina marginata*, *Cavarotalia annectens*, and *Uvigerina canariensis*. There are some planktonic foraminiferal assemblages, such as *Globigerina* sp. Foraminiferal assemblages were identified as mixed burial groups, which are characteristic of in situ and alien species. In situ species are dominated by nearshore euryhaline species, such as *A. beccarii* vars. and *A. convexidorsa*. Meanwhile, several alien open-sea species were identified, such as *E. naraensis*, *H. nipponica*, and *U. canariensis*. Moreover, some species living in deeper water (>20 m deep) are also identified, including *A. compressiuscula*, *B. marginata*, and *B. robusta*.

Based on chronostratigraphic sequence and paleontological assemblage analysis, we divide the marine sediment layers of Core YZ07 into the Holocene transgression (MT 1), MIS 3 transgression (MT 2), and MIS 5 transgression (MT 3), illustrating at least three terrestrial-marine sedimentary cycles in the study area since the Late Pleistocene.

4.3 Sedimentary environments on lithostratigraphic and chronostratigraphic sequences

According to the sedimentary facies, ^{14}C and OSL dating, and corresponding oxygen isotope stage (from MIS 6 to MIS 1), borehole sediments can be divided into 6 units from bottom to top (Figure 2).

4.3.1. Prior to late Mid-Pleistocene unit (150.0–72.1 m)

The OSL dates at the core depths of 70.4, 80.1, 91.2, and 100 m show an age of >100 ka BP. Therefore, it is likely that the bottom sediment age is equivalent to MIS 6 (ca. 128–180 ± 20 ka BP) or older (Lowe and Walker, 1997; Lisiecki and Raymo, 2005). Based on lithology, erosional contact, and paleontological analysis and dating, this unit is interpreted to have been deposited in a terrestrial environment, corresponding to the late Mid-Pleistocene stage or ages beyond from bottom to top.

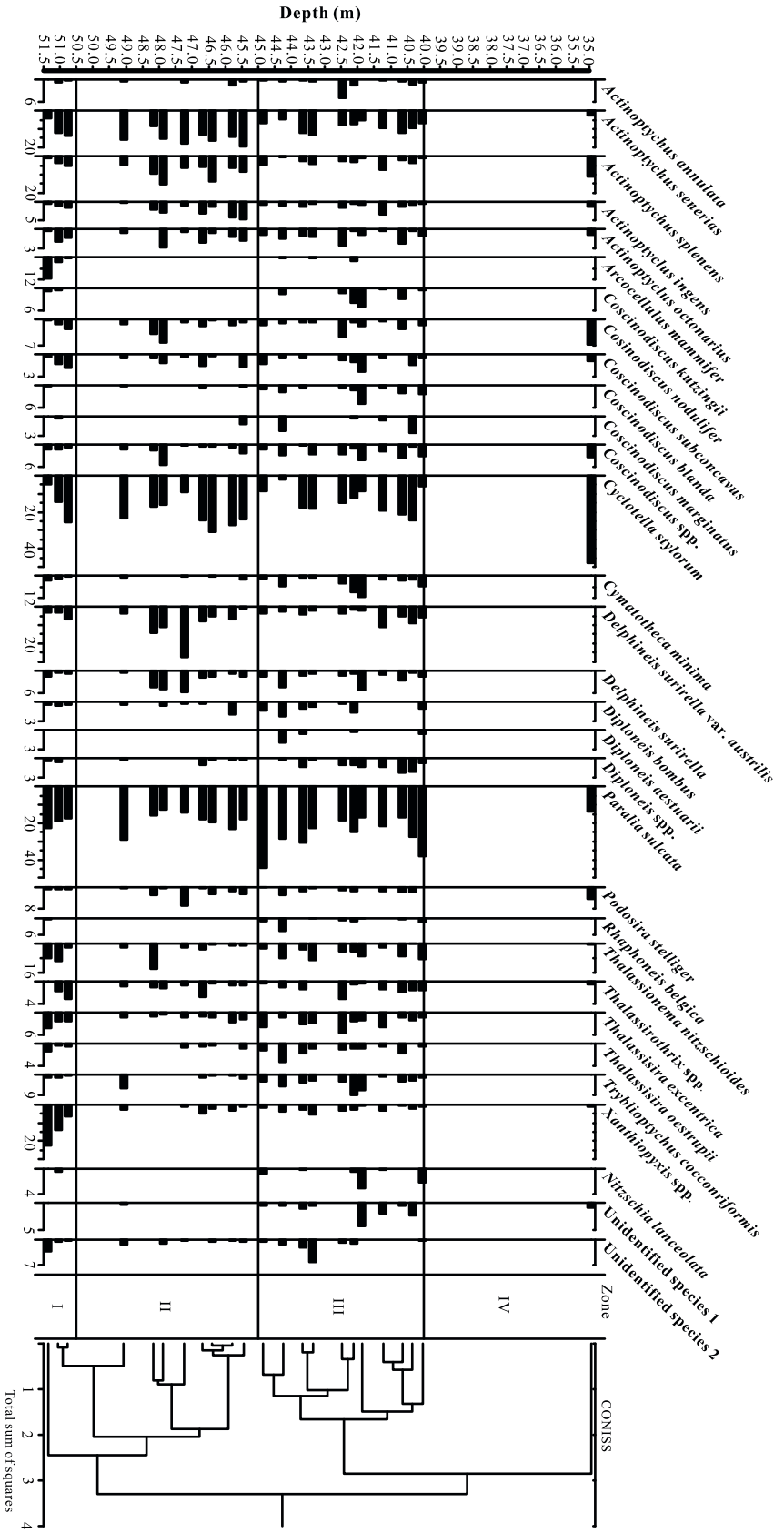

Figure 3. Relative abundance of the dominant diatom taxa in YZ07.

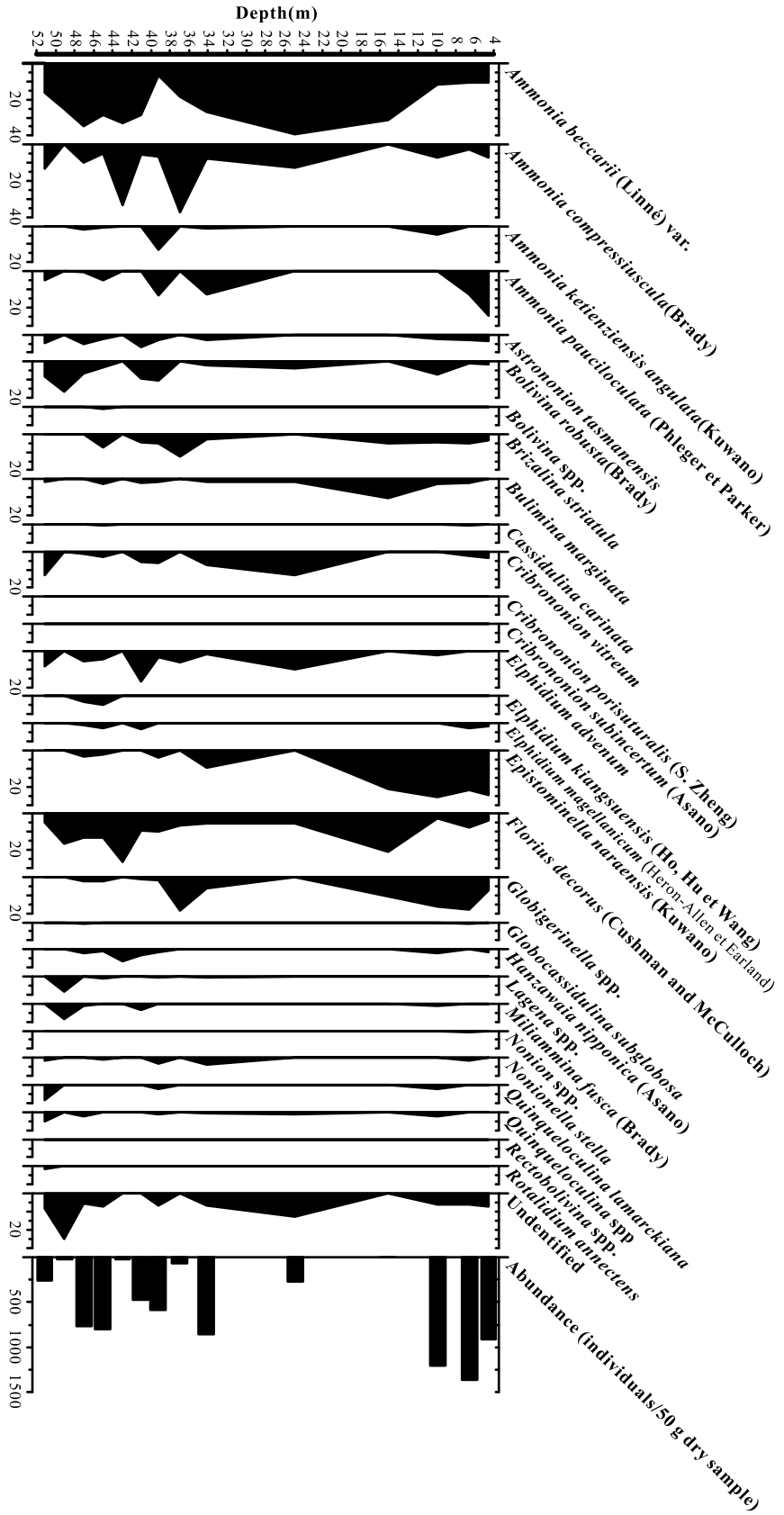

Figure 4. Relative abundance of the dominant foraminiferal taxa in YZ07.

Table 4. Abundance of foraminiferal assemblages and types down the core of YZ07.

Sample no.	Depth(m)	Abundance (individuals/50 g dry sediments)	Planktonic species (%)	Benthic species (%)
A-042	–4.55	9129	8.9	91.1
A-058	–6.56	13590	18.2	81.8
A-090	–9.9	12090	16.2	83.8
A-142	–15.12	34	8	92
A-238	–24.87	2723	0	100
A-338	–34.17	8513	6.4	93.6
A-356	–36.99	749	0	100
A-373	–39.25	5864	3.04	96.96
A-397	–41.07	4747	1.52	98.48
A-416	–42.96	257	0	100
A-437	–45.05	7967	1.94	98.06
A-457	–47.04	7677	0.05	99.95
A-477	–49.07	300	2.1	97.9
A-495	–51.15	2568	1.15	98.85
A-580	–59.72	13589	–	–
A-630	–65.05	517	–	–
A-686	–70.967	245	–	–

4.3.2. The early Late Pleistocene unit (72.10–54.98 m)
Both ^{14}C dates at the core depths of 56.06 and 62.82 m show an age of >47 ka BP and one OSL date at the core depth of 70.4 m shows an age of >100 ka BP. This unit is estimated to be ca. 73–128 ka BP, corresponding to MIS 5 (Martinson et al., 1987; Lambeck and Chappell, 2001). The sediments of this unit show a rise in sea level of the SYS based on a transition of sedimentary facies from river-mouth to littoral deposits from the bottom to top, which suggests that this unit was deposited in a marine environment during MIS 5 (MT 3), when marine transgression events were also recorded in the other cores of the SYS (c.f. Zhao et al., 2008).

4.3.3. The mid-Late Pleistocene unit (54.98–52.16 m)
According to the sedimentary facies and chronostratigraphic sequence, this unit (54.98–52.16 m) is interpreted to have been deposited in a terrestrial environment during the mid-Late Pleistocene, corresponding to MIS 4 sea-level lowstands (Lowe and Walker, 1997; Lisiecki and Raymo, 2005).

4.3.4. The late Late Pleistocene unit (52.16–43.88 m)
Radiocarbon and OSL dates at the core depths of 43.88 m and 50 m show ages of 25663 ± 104 cal. a BP and 26.20 ± 3.5 ka BP, respectively. The age of the unit is estimated to be later MIS 3 (Lowe and Walker, 1997; Lambeck and Chappell, 2001; Lisiecki and Raymo, 2005). The unit is interpreted to have been deposited in a littoral environment, which suggests a rise in sea level of the SYS during later MIS 3 (MT 2), when a marine transgression event was recorded in the other cores of the SYS (c.f. Zhao et al., 2008; Wang et al., 2013).

4.3.5. The Holocene unit (0–43.88 m)
Radiocarbon dates in this unit range between 3175 ± 35 and 11,298 ± 46 cal. a BP. This unit is interpreted to reflect several transitions of sedimentary environments from a coastal area to an estuarine/littoral area, then to a tidal-flat environment in response to a postglacial sea-level rise. The unit is equivalent to the MIS 1 marine transgression (MT 1) (Holocene, 12 ± 1.5 cal. ka BP; Lowe and Walker, 1997).

Overall, sedimentary, paleontological, and chronostratigraphic analyses suggest that the stratigraphic sequence of the study area inferred from YZ07 can be divided into six stages (MIS 1–MIS 6), and the sedimentary facies are dominated by interbedded marine and terrestrial deposits, including 7 layers of terrestrial deposits (floodplain, fluvial, and lacustrine facies), 4 layers of marine deposits (tidal-flat, neritic, and littoral facies), and 3 layers of marine-terrestrial transitional deposits (estuarine facies). The burial depths of the basal boundary during MIS 1, MIS 3, MIS 4, and MIS 5 in this region inferred from YZ07 were at the depths of 43.88 m, 52.16 m, 54.98 m, and 72.1 m, respectively.

5. Discussion

5.1. Implications of major sedimentary environment evolution since MIS 5

The lithology, paleontological fossils, and ^{14}C and OSL dating in YZ07 and the 12 collected cores suggest that three significant marine transgressions (MT 3, MT 2, and MT 1), together with two marine regressions during MIS 4 and MIS 2, occurred in the SYS since MIS 5 (Figure 5), which corresponds perfectly to three sea-level highstands and two sea-level lowstands of the worldwide coasts from MIS 5 to MIS 1 (Wang et al., 1981).

The bottom boundary of the MIS 1 sediments in Core YZ07 was determined to be 44 m based on a number of AMS ^{14}C and OSL dates. Previous studies indicate that the bottom boundary of MIS 1 sediments in the study area mainly ranges from 15 m to 29 m in depth (Wang et al., 2012; Li and Yin, 2013; Xia et al., 2013; Zhang et al., 2014; Wang et al., 2014a; Ji et al., 2015; Sun et al., 2015). In addition, due to the subaerially exposed continental shelf and subsequent pedogenesis process in the SYS during MIS 2, the brownish yellow stiff clay layer (termed "desiccated crust" by Yim et al., 1990 and "paleosol" by Li et al., 2002) has almost become an important regional marker bed of MIS 2 in the study area (Chen et al., 2008). The ^{14}C dates at the core depths of 42.96 m and 43.88 m show ages of 11,298 ± 46 cal. a BP and 25,663 ± 104 cal. a BP, respectively, which suggests that there is a great sedimentary hiatus from later MIS 3 to MIS 1. Therefore, stiff clay layers in MIS 2 were considered to be missing in Core YZ07. An alternative explanation is that the cores were in a paleo-river channel and that sediments during MIS 2 were scoured away by terrestrial rivers. Another explanation is that an erosional marine transgression in the early Holocene probably created the sedimentary hiatus of MIS 2 (Sun et al., 2015). Afterwards, those cores were filled by subsequent huge quantities of sediments from terrigenous rivers during the Holocene as the sea level rose. Three patterns of sea levels during the later MIS 3 were inferred from salt-water diatom assemblages of YZ07, which suggests that the sea levels vary from the high to the slightly low to the high during MIS 3. In addition, MIS 4 sediments in YZ07 were thin (2.7 m in thickness), and the upper layer of MIS 4 sediments exhibits an obvious erosional contact with overlying sediments during MIS 3 (Figure 2), which suggests that there is also a depositional hiatus during MIS 4. Sediments during MIS 5 are interpreted to have been deposited in a marine environment. However, thick sediments (72.10–150 m in YZ07) during MIS 6 or older are interpreted to have been deposited in a terrestrial environment. Therefore, the advent of MIS 5 reflects a great shift in depositional environments from terrestrial to marine deposits in the study area.

The western SYS has experienced several alternations of terrestrial to marine environments since MIS 5, including land-sea transitional environments, which can be obviously observed by the transitions of sedimentary facies in Core YZ07. There are in total 78-m-long terrestrial sediments (fluvial/lacustrine/floodplain facies) in Core YZ07, which accounts for 52% of the core. Terrestrial sediments in Core YZ07 were primarily deposited in MIS 4 and MIS 6 or beyond. Moreover, marine sediments (tidal-flat/littoral/neritic facies) are totally 46.5 m in length, accounting for 31% of the core, and the sediments were primarily deposited during MIS 5, later MIS 3, and MIS 1. The sedimentary record inferred from Core YZ07 indicated that the SYS has undergone major depositional environmental transitions from land to sea via a unique time point from the later Mid-Pleistocene to the early Late Pleistocene. Just under river–sea interactions of two large terrestrial rivers (the paleo Yellow River and paleo Yangtze River) and marine hydrodynamics of the SYS, land–sea transitional sediments (estuarine/deltaic facies) accumulated in tidal flats of the Jiangsu coast. Transitional sediments are in total 25.5 m long in YZ07, accounting for 17% of the core. The transitional environments reflected from Core YZ07 partly coincide with previous viewpoints that the continental shelf of the Chinese marginal sea was once a coastal plain during the Late Pleistocene, and an aggradational continental shelf and a coastal-estuarine-deltaic system have been developed by receiving massive terrigenous sediments (Wang, 2002; Wang et al., 2006; Wang, 2014).

5.2. Comparison of MIS 3 and MIS 5 marine sediments

The data of 12 regional cores, together with Core YZ07, in the coastal plains and nearshore area of the SYS were compiled in terms of lithology, stratigraphy, chronology, and paleontological fossils (Figure 5). Most of the cores are relatively short, and the bottom of the cores was confined to MIS 3. However, there are precise OSL dates in 5 cores (WJ, QP88, SG7, FX, and MFC), and the longest OSL dates for these cores were dated back to 100 ± 8 to 134 ± 11 ka BP, which is correlative with MIS 5 or older. Based on a comparison of the sedimentary facies and chronostratigraphic sequence with the above 5 cores, the marine sediments of 72.10–54.98 m in Core YZ07 are estimated to be MIS 5 sediments. As indicated in Figure 5, later MIS 3 marine transgression events were recorded in all 13 cores, of which 6 cores (ZK04, WJ, QP88, SG7, MFC, and YZ07) indicated a sea-level highstand during MIS 5.

Some 20–30 m of thickness of the MIS 3 coastal sediments are generally found in many boreholes in the offshore area and adjacent deltaic plain of the SYS (Zhao et al., 2008), which is only consistent with some cores, such as 07SR03, 11DT02, MFC, ZK04, and BY1 (Figure 5). In contrast, thin layers (8–18 m) of MIS 3 marine sediments seem to appear more in boreholes,

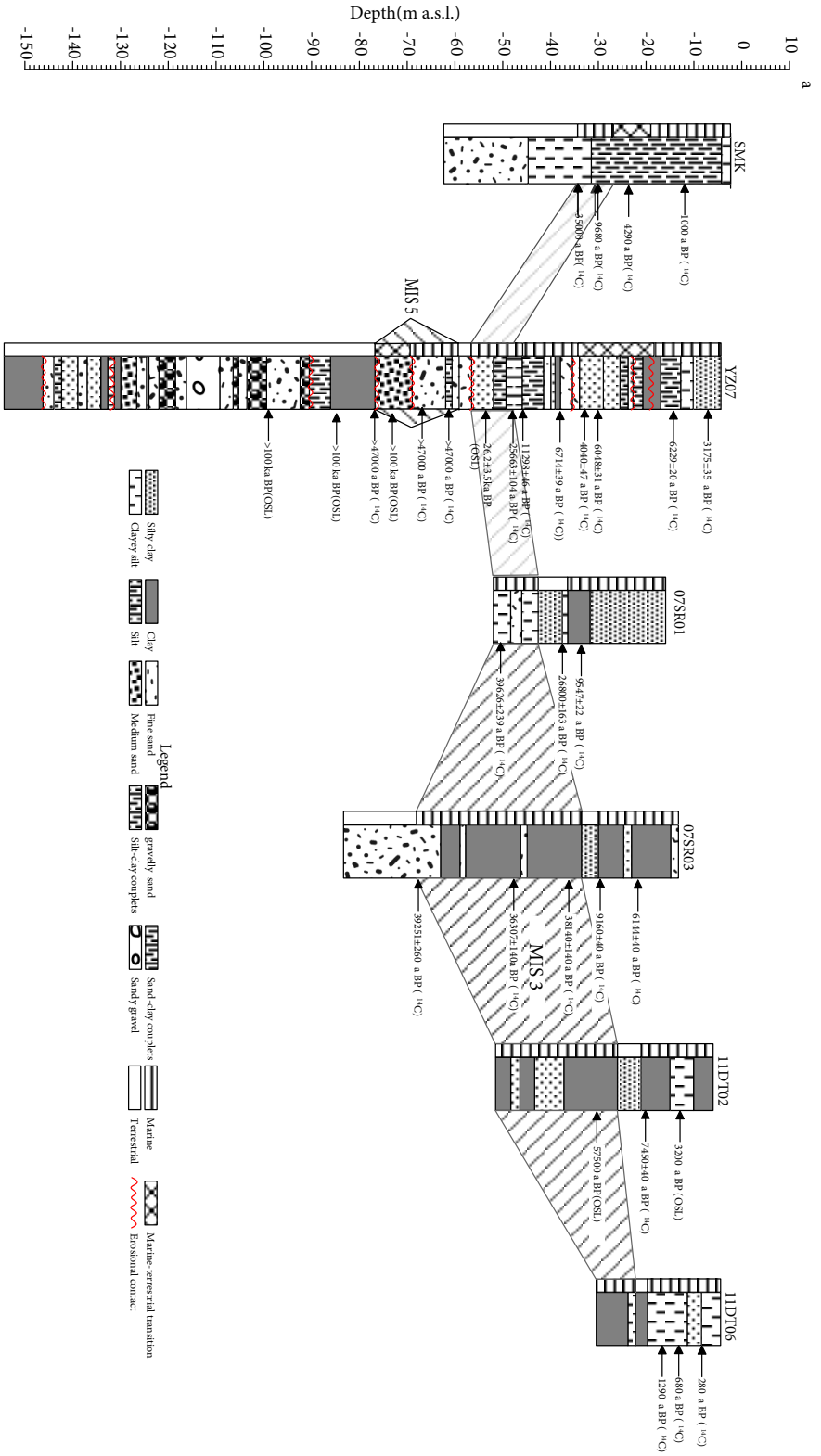

Figure 5. Regional comparison of MIS 3 and MIS 5 transgressions in the offshore area of the South Yellow Sea (a) and adjacent deltaic plain (b). Core references: 07SR03 (Zhang et al., 2014); 07SR01 (Xia et al., 2013); 11DT02 (Li et al., 2013); 11DT06 (Wang et al., 2014); SMK (Zhu et al., 1999); BY1 (Zhang et al., 2010); ZK04 (Zhong et al., 1999); WJ (Wang et al., 2013); QP88 (Wang et al., 2013); FX (Zhao et al., 2008); MFC (Zhao et al., 2008); SG7 (Wang et al., 2013); YZ07 (this study).

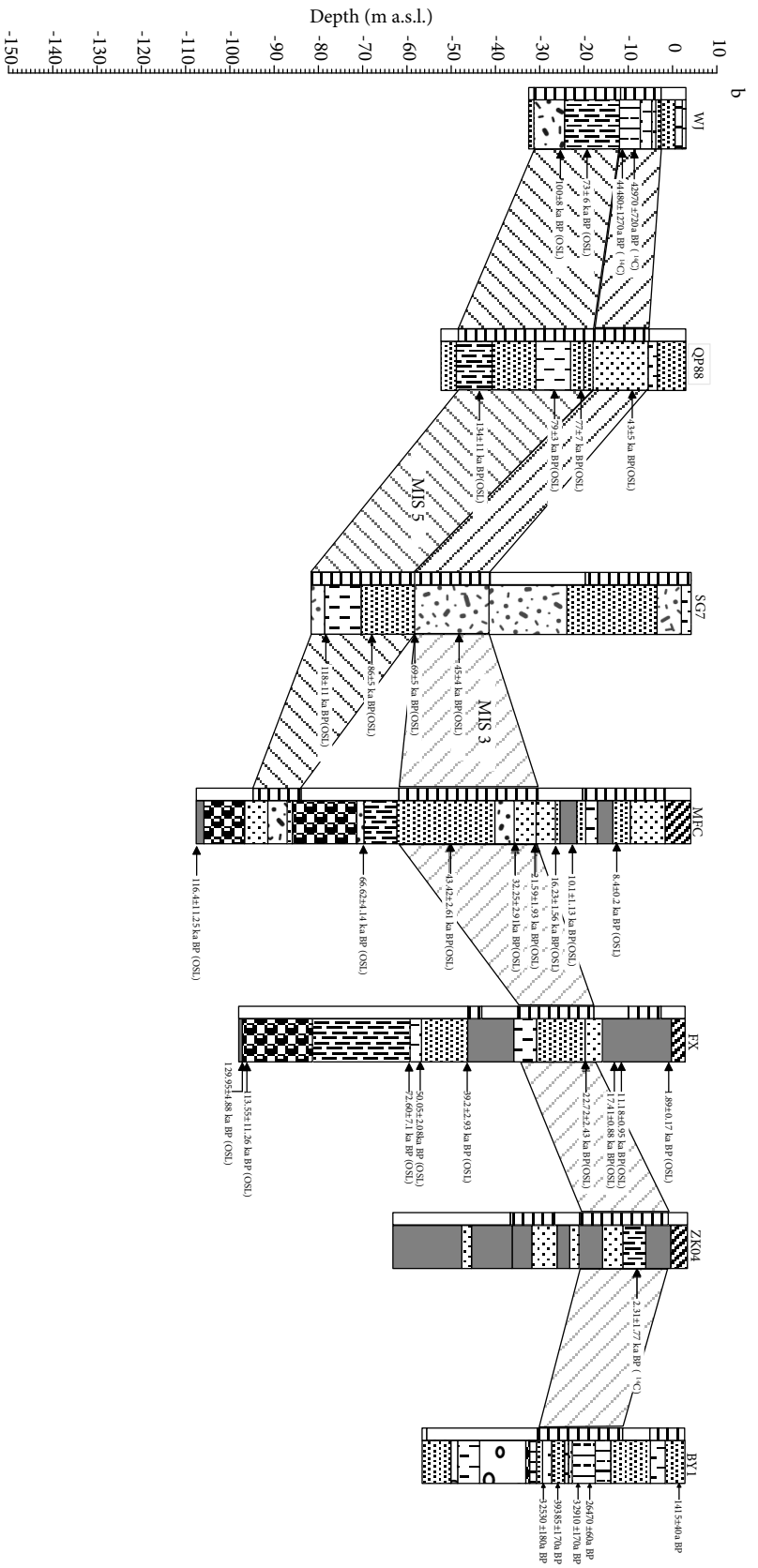

Figure 5. (Continued).

such as cores YZ07, SMK, 07SR01, WJ, QP88, SG07, and FX (Figure 5). The comparisons indicate that cores are located closer to the present shoreline landward, and the burial depths of the upper boundary of marine sediments during MIS 3 are relatively deeper (–28 to –46 m a.s.l.). In contrast, the burial depths become shallower (–2 to –19 m a.s.l.) in cores that are located farther away from the present shoreline landward. In addition, previous studies suggested that there was a sporadic distribution of marine sediments in the SYS during MIS 5, when the study area was primarily under land–sea transitional environments (deltaic or estuarine facies), and the burial depths of sediments in MIS 5 were at –85 to –105 m a.s.l. with a thickness of <10 m (Wang et al., 1981; Zhao et al., 2008). After the comparisons of some published core data in the SYS, we conclude that MIS 5 sediments are actually scattered sporadically, but the scopes of the burial depths and the thickness of MIS 5 sediments vary more widely, which are estimated to be –69 to –104 m a.s.l. and 9.4–30 m, respectively. It also suggests that most of those MIS 5 sediments were deposited in a marine environment (Figure 5). It is likely that the thickness and burial depths of marine sediments are the result of glacioeustatic change, sediment compaction, terrigenous sediment inputs, and neotectonic activity based on the dynamic simulation of transgression (Ye et al., 2016).

The timing of MT 2 (or MIS 3 transgression) has been heatedly debated in recent years (Yi et al., 2013). The MIS 3 transgression was supposed to be not in existence and the previously radiocarbon-dated MIS 3 transgression should be adjusted to MIS 5 by OSL dating method in the South Bohai Sea, China (Chen et al., 2008; Yi et al., 2013) and in the Gulf of Mexico (Simms et al., 2009). Previous studies proposed that radiocarbon dates had a young age bias and the 'MIS 3 transgression' was significantly underestimated (Yim et al., 1990; Long and Shen, 2015), so the discrepancy on the timing of MT 2 was likely to be related to the dating difference between the radiocarbon and OSL methods (Yi et al., 2013). However, ^{14}C and OSL dates at the core depths of 43.88 m and 50 m in Core YZ07 show ages of 25,663 ± 103 cal. a BP and 26.20 ± 3.5 ka BP, respectively (Figure 2). Meanwhile, salt-water diatom and foraminifera assemblages were also found during MIS 3. Thus, marine transgression during MIS 3 inferred from Core YZ07 is confirmed based on paleontological fossils and ^{14}C and OSL dating. In addition, MIS 3 transgression events were widely reported based on many cores drilled from both deltaic plain (c.f. Zhong et al., 1999; Zhao et al., 2008; Zhang et al., 2010; Wang et al., 2013) and offshore borehole cores (c.f. Zhu et al., 1999; Li et al., 2013; Xia et al., 2013; Wang et al., 2014; Zhang et al., 2014; Ji et al., 2015; Sun et al., 2015) in the SYS (Figure 5). Sediment samples for 5 cores around the SYS were dated to an age range of 26 ka to 49 ka BP by the OSL dating method, which were obviously constrained to MIS 3 (Figure 5). It is likely that regional tectonic movement may partially lead to the discrepancy of the MIS 3 transgression in different regions (Wang and Wang, 1980; Wang and Tian, 1999). Although the highest sea levels during MIS 5 are considered to be higher than those during MIS 3 in the marginal seas of China, there is still a puzzle why the spatial distribution of MIS 3 marine sediments is wider than that of MIS 5. The presence of foraminifera in the strata is commonly regarded as robust paleontological evidence of transgressions. If no or few foraminifera are found in the strata, there may be false impressions that the transgression is not in existence or is weak. Currently, the conclusion that the spatial distribution and thickness of MIS 3 marine sediments are generally greater than MIS 5 ones in the western SYS is just based on foraminifera and ostracodes (Wang et al., 1981). One possible interpretation for the scarcity of foraminifera during MIS 5 is that the study area was dominated by many local rivers developed with abundant freshwater and massive sediments, and forams and ostracodes may not have survived in the water of low salinity and high turbidity (Zhao et al., 2008). In addition, the MIS 5 climate in the SYS is more humid with more abundant precipitation according to pollen analysis (Wang et al., 1981). Wang et al. (1981) further stated that the topography of the east coasts of China during MIS 5 fluctuated more drastically than that of the present and a more deeply incised valley formed, so that sea water could intrude into continental areas along many valleys with sporadically lateral distributions. This indicates that MIS 5 marine sediments are easily present in paleo-river channels or around them. Therefore, another alternative explanation is that the flattened relief of the study area and lagoon-sand bar environments' lack of freshwater supply during MIS 3 seemed to make the MIS 3 transgression more significant, while a high relief and large amounts of runoff during MIS 5 resulted in part of the MIS 5 transgression sediments being scoured away (Zhao et al., 2008; Wang et al., 2008). The aforementioned explanations actually focus on two main factors of transgression pattern discrepancy, i.e. climate and regional neotectonic movement, both of which could explain why the spatial distribution of MIS 5 marine sediments are more limited than that of MIS 3. Therefore, we conclude that climate and regional tectonic activity may be the mechanisms of the discrepancy between the Late Pleistocene transgressions, of which dominant factors are the changes of climate-driven glaciers.

Overall, sedimentological analysis, grain size, and paleontological fossils of Core YZ07 demonstrated that the western SYS was dominated by alternating fluvial and

marine deposits since MIS 5. Three marine transgressions (MIS 5, MIS 3, and the Holocene transgressions) from MIS 5 to MIS 1 in the western SYS were confirmed based on the marine sediments in Core YZ07 and a range of published cores, while a major sedimentary hiatus occurred during MIS 2 or MIS 4 probably because of strong erosion from a terrigenous river or marine transgression. Above all, MIS 3 marine transgression in the SYS has been confirmed by the analysis of different dating methods (OSL and AMS ^{14}C) and paleontological fossils. Furthermore, the intensity of marine transgression and the height of sea levels during MIS 3 and MIS 5 recorded in sediments are dominated by the changes of climate-driven glaciers and regional tectonic activity.

Acknowledgments

This research was funded by the National Basic Research Programs of China (Grant no.: 2013 CB 956501 and 2012CB956103); Cultivation Fund Project of College of Environmental Science and Engineering, Anhui Normal University (Grant no.: CFP201707); National Key R&D Program (Silting-up Control and Functional Restoration of Reservoirs and Lakes); International Cooperation Program of Chinese Academy of Sciences (Grant no.: KZZD-EW-TZ-08); and Anhui Provincial Natural Sciences Foundation (No. 1708085MC59). We are grateful to Professors Feng Gui (Zhejiang Marine University), Yong Yin, and Shu Gao (Nanjing University) for their support and help in coring and sample analysis.

References

Bureau of Geology and Mineral Resources of Jiangsu (1984). Regional Geological Log of Jiangsu and Shanghai. Beijing, China: Geological Publishing House (in Chinese).

Chappell J (1974). Geology of coral terraces, Huon Peninsulla, New Guinea: a study of Quaternary tectonic movements and sea level changes. Geol Soc Am Bull 85: 553-570.

Chappell J, Shackleton NJ (1986). Oxygen isotopes and sea level. Nature 324: 137-140.

Chappell J, Veeh HH (1978). Late Quaternary tectonic movements and sea-level changes at Timor and Atauro Island. Geol Soc Am Bull 89: 356-368.

Chen J (1957). Notes on the development of the Yangtze estuary. Acta Geogr Sin 23: 241-253 (in Chinese with English abstract).

Chen YK, Li ZH, Shao YX, Wang ZS, Gao WP, Yang XL (2008). Study on the Quaternary chronostratigraphic section in Tianjin Area. Seismol Geol 30: 383-399 (in Chinese with English abstract).

Fuji N, Horowitz A (1989). Brunch epoch palaeoclimates of Japan and Israel. Palaeogeogr Palaeoclimatol Palaeoecol 72: 79-88.

Gao S (2013). Holocene shelf-coastal sedimentary systems associated with the Changjiang River: An overview. Acta Oceanol Sin 32: 4-12.

Gao S, Collins MB (2014). Holocene sedimentary systems on continental shelves. Mar Geol 352: 268-294.

Gersonde R, Zielinski U (2000). The reconstruction of late Quaternary Antarctic sea ice distribution —the use of diatoms as a proxy for sea ice. Palaeogeogr Palaeoclimatol Palaeoecol 162: 263-286.

Huang ZG, Li PR, Zhang ZY (1986). Sea Level Changes in the South China Since the Late Pleistocene. Beijing, China: Ocean Publishing House (in Chinese).

Jacobs Z (2008). Luminescence chronologies for coastal and marine sediments. Boreas 37: 508-535.

Ji Y, Yin Y, Li Q, Wang AH (2015). The core-recorded strata and environmental changes since the Late Pleistocene in Kushuiyang area of the radial ridge system, Jiangsu offshore, southern Yellow Sea. J Nanjing Univ (Natural Sciences) 51: 641-657 (in Chinese with English abstract).

Kim JC, Cheong D, Shin S, Park YH, Hong SS (2015). OSL chronology and accumulation rates of the Nakdong deltaic sediments, southeastern Korean Peninsula. Quat Geochronol 30: 245-250.

Lai ZP, Mischke S, Madsen D (2014). Paleoenvironmental implications of new OSL dates on the formation of the "Shell Bar" in the Qaidam Basin, northeastern Qinghai–Tibetan Plateau. J Paleolimnol 51: 197-210.

Lambeck K, Chappell J (2001). Sea level change through the last glacial cycle. Science 292: 679-686.

Li CX, Wang P, Sun HP, Zhang JQ, Fan DD, Deng B (2002). Late Quaternary incised-valley fill of the Yangtze delta (China): its stratigraphic framework and evolution. Sediment Geol 152: 133-158.

Li Q, Yin Y (2013). Sedimentary facies and evolution of the Likejiao sandy ridge, in the South Yellow Sea offshore area, eastern China. Geogr Res 32: 1843-1854 (in Chinese with English abstract).

Lin CM, Zhang X, Xu ZY, Deng CW, Yin Y, Cheng QQ (2015). Sedimentary characteristics and accumulation conditions of shallow biogenic gas for the late Quaternary sediments in the Yangtze River delta area. Adv Earth Sci 30: 589-601 (in Chinese with English abstract).

Lin JX, Zhang SL, Qiu JB (1989). Quaternary marine transgressions and paleoclimate in the Yangtze River delta region. Quat Res 32: 296-306.

Lisiecki LE, Raymo ME (2005). A Pliocene-Pleistocene stack of 57 globally distributed benthic $\delta^{18}O$ records. Paleoceanography 20: 1-17.

Long H, Shen J (2015). Underestimated ^{14}C-based chronology of late Pleistocene high lake-level events over the Tibetan Plateau and adjacent areas: Evidence from the Qaidam Basin and Tengger Desert. Sci Chin-Earth Sci 58: 183-194.

Lowe JJ, Walker MJC (1997). Reconstructing Quaternary Environments. 2nd ed. Harlow, UK: Addison Wesley Longman Press.

Martinson DG, Pisias WG, Hays J, Imbrie J, Moore TC, Shackleton NJ (1987). Age dating and the orbital theory of the ice age: development of a high resolution 0 to 300,000 year chronostratigraphy. Quat Res 27: 1-29.

Murray AS, Wintle AG (2000). Luminescence dating of quartz using an improved single-aliquot regenerative- dose protocol. Radiat Meas 32: 57-73.

Murray-Wallace CV (2002). Pleistocene coastal stratigraphy, sea-level highstands and neotectonism of the southern Australian passive continental margin — a review. J Quat Sci 17: 469-489.

Prescott JR, Hutton JT (1994). Cosmic ray contribution to dose rates for luminescence and ESR dating: large depths and long-term time variations. Radiat Meas 23: 497-500.

Ren ME (1986). Comprehensive Surveys of Coastal Zones and Tidal Flat Resources in Jiangsu. Beijing, China: Ocean Press (in Chinese).

Schrader HJ, Gersonde R (1978). Diatoms and silicoflagellates. In: Zachariasse WJ, editor. Micropaleontological Methods and Techniques — An Exercise on an Eight Metres Section of the Lower Pliocene of Capo Rossello, Sicily. Utrecht, the Netherlands: Utrecht Micropaleontological Bulletins, pp. 129-176.

Shi YF, Yu G (2003). Feature and mechanism of warm-humid climate and sea transgression in the 40~30ka BP in China. Quat Sci 23: 1-11 (in Chinese with English abstract).

Shi YF, Yu G, Liu XD, Li BY, Yao TD (2001). Reconstruction of the 30–40 ka BP enhanced Indian monsoon climate based on geological records from the Tibetan Plateau. Palaeogeogr Palaeoclimatol Palaeoecol 169: 69-83.

Simms AR, DeWitt R, Rodriguez AB, Lambeck K, Anderson JB (2009). Revisiting marine isotope stage 3 and 5a (MIS3–5a) sea levels within the northwestern Gulf of Mexico. Global Planet Change 66: 100-111.

Steinen RP, Harrison RS, Matthews RK (1973). Eustatic low stand of sea level between 125,000 and 105,000 B.P.: evidence from the subsurface of Barbados, West Indies. Geol Soc Am Bull 84: 63-70.

Sugisaki S, Buylaert JP, Murray AS, Tsukamoto S, Nogi Y, Miura H, Sakai S, Lijima K Sakamoto T (2010). High resolution OSL dating back to MIS 5e in the central Sea of Okhotsk. Quat Geochronol 5: 293-298.

Sun ZY, Li G, Yin Y (2015). The Yangtze River deposition in southern Yellow Sea during Marine Oxygen Isotope Stage 3 and its implications for sea-level changes. Quat Res 83: 204-215.

Wang JT, Wang PX (1980). Relationship between sea–level changes and climatic fluctuations in East China since Late Pleistocene. Acta Geogr Sin 35: 299-312 (in Chinese with English abstract).

Wang PX, Min QB, Bian YH, Chen XR (1981). Strata of Quaternary transgression in East China: a preliminary study. Acta Geol Sin 1: 1-13 (in Chinese with English abstract).

Wang Q, Tian G (1999). The Neotectonic setting of late Quaternary transgressions on the eastern coastal plain of China. J Geomech 5: 41-48 (in Chinese with English abstract).

Wang Y (1998). Sea-level changes, human impacts and coastal responses in China. J Coast Res 14: 31-36.

Wang Y (2002). Radial Sand Ridges of the Continental Shelf of the Yellow Sea. Beijing, China: Environmental Science Press (in Chinese).

Wang Y (2014). Environment and Resources of Radial Sand Ridges in the Southern Yellow Sea. Beijing: Ocean Press (in Chinese).

Wang Y, Zhang Y, Zou X, Zhu D, Piper D (2012). The sand ridge field of the South Yellow Sea: Origin by river–sea interaction. Mar Geol 291-294: 132-146.

Wang Y, Zhang ZK, Zhu DK, Yang JH, Mao LJ, Li SH (2006). River–sea interaction and the north Jiangsu Plain formation. Quat Sci 26: 301-320 (in Chinese with English abstract).

Wang Y, Zhu DK, Zhou LF (1998). Sedimentary features and evolution of the radial sand in the South Yellow Sea. China Sci (D-Series) 8: 385-393 (in Chinese).

Wang YH, Yin Y, Xia F, Zou XQ (2014). Characteristics of sedimentary strata and environmental changes of Kushuiyang tidal channel in the radial tidal ridge field, southern Yellow Sea. J Nanjing Univ (Natural Sciences) 50: 564-575 (in Chinese with English abstract).

Wang ZH, Jones B, Chen T, Zhao BC, Zhan Q (2013). A raised OIS 3 sea level recorded in coastal sediments, southern Changjiang delta plain, China. Quat Res 79: 424-438.

Wang ZH, Zhao BC, Chen J, Li X (2008). Chronostratigraphy and two transgressions during the Late Quaternary in Changjiang delta area. J Paleogeogr 10: 99-110 (in Chinese with English abstract).

Webb T 3rd (1985). A global climate data base for 6000 yr BP. US DOE/EV/10097-6. Washington, DC, USA: US Department of Energy.

Xia F, Zhang YZ, Wang Q, Ying Y, Wegmann KW, Liu JP (2013). Evolution of sedimentary environments of the middle Jiangsu coast, South Yellow Sea since late MIS 3. J Geogr Sci 23: 883-914.

Yang SY, Jung H, Lim D, Li CX (2003). A review on the provenance discrimination of sediments in the Yellow Sea. Earth-Sci Rev 63: 93-120.

Yao Z, Guo Z, Xiao G, Wang Q, Shi X, Wang X (2012). Sedimentary history of the western Bohai coastal plain since the late Pliocene: Implications on tectonic, climatic and sea-level changes. J Asian Earth Sci 54/55: 192-202.

Ye LT, Yu G, Liao MN, Li YF (2016). Dynamic simulations of transgressions along Fujian and Jiangsu coasts during the later MIS 3. Acta Oceanol Sin 10: 1-14.

Yi L, Lai ZP, Yu HJ, Su Q, Yao J, Wang X, Shi X (2013). Chronologies of sedimentary changes in the south Bohai Sea, China: constraints from luminescence and radiocarbon dating. Boreas 43: 267-284.

Yim WWS, Ivanovich M, Yu KF (1990). Young age bias of radiocarbon dates in pre-Holocene marine deposits of Hong Kong and implications for Pleistocene stratigraphy. Geo-Mar Lett 10: 165-172.

Zhang J, Tsukamoto S, Grube A, Frechen M (2014). OSL and ^{14}C chronologies of a Holocene sedimentary record (Garding-2 core) from the German North Sea coast. Boreas 43: 856-868.

Zhang X, Ge CD, Yin Y, Lv YM, Li HQ (2014). The geochemical characteristics and sedimentary environment evolution of the Dabeicao channel and Dongsha shoal area among the radial tidal sand ridge system, southern Yellow Sea. J Nanjing Univ (Natural Sciences) 50: 538-552 (in Chinese with English abstract).

Zhang ZK, Xie L, Zhang YF, Xu J, Li SH, Wang Y (2010). Sedimentary records of the MIS 3 transgression event in the north Jiangsu plain, China. Quat Sci 30: 883-891 (in Chinese with English abstract).

Zhao BC, Wang ZH, Chen J, Chen ZY (2008). Marine sediments records and relative sea level change during late Pleistocene in the Changjiang delta area and adjacent continental shelf. Quat Int 186: 164-172.

Zhong SL, Liu JL, Li XX, Mu XN, Zou SM, Liu ZP, Zhu ZY (1999). Preliminary study of biota and environments since late Pleistocene in the Tai-Ge area, southern Jiangsu province, China. Acta Micropalaeontol Sin 16: 167-180 (in Chinese with English abstract).

Zhu XD, Ren ME, Zhu DK (1999). Changes in depositional environments in the area near the centre of the North Jiangsu radial banks since the Late Pleistocene. Oceanol Limnol Sin 30: 427-434 (in Chinese with English abstract).